Thermoelectric properties of p-type polycrystalline $Bi_{0.8}Sb_{0.8}In_{0.4}Se_3$

Feng Jiang[1,2], Chengliang Xia[2], Yongbin Zhu[1], Zhijia Han[1], Chengyan Liu[3], Jiating Xia[1], Yue Chen[2*], and Weishu Liu[1*]

AFFLIATIONS

[1]Department of Materials Science and Engineering, Southern University of Science and Technology, Shenzhen 518055, Guangdong, China

[2]Department of Mechanical Engineering, The University of Hong Kong, Pokfulam Road, Hong Kong SAR, China

[3]Department of Physics, Southern University of Science and Technology, Shenzhen 518055, Guangdong, China

Authors to whom correspondence should be addressed: liuws@sustech.edu.cn (Weishu Liu), yuechen@hku.hk (Yue Chen).

ABSTRACT

Achieving both n-type and p-type performance in one thermoelectric material family is of great benefit for the thermoelectric device due to the comparable mechanical properties. Bi_2Se_3 shows strong n-type behavior due to the intrinsic Se vacancy. Herein, we successfully synthesized p-type poly-crystalline $Bi_{0.8}Sb_{0.8}In_{0.4}Se_3$, which has the same crystalline structure as Bi_2Te_3, with an intrinsic Seebeck coefficient of 500 $\mu V\ K^{-1}$ at room temperature. It is found that Mn is a good p-type charge carrier provider in the as-fabricated $Bi_{0.8}Sb_{0.8}In_{0.4}Se_3$ thermoelectric material. An optimized power factor of ~420 $\mu W\ m^{-1}\ K^{-2}$ and a low thermal conductivity of 0.51 $W\ m^{-1}\ K^{-1}$ result in a ZT of 0.48 at 350 °C in $Mn_{0.03}Bi_{0.77}Sb_{0.8}In_{0.4}Se_3$. Our work provides a new insight into the manipulation of the intrinsic defects via high entropy strategy.

Main Text

Bi_2Se_3 shows intrinsically strong n-type behavior due to the low defect formation energy of Se vacancy[1,2] and high saturation vapor pressure of Se in the sintering process.[3] The relative low carrier mobility results in the inferior n-type performance as compared with Bi_2Te_3. Nevertheless, Park and Singh predicted that hole-doped Bi_2Se_3 material could have potential better performance at medium temperature as compared with Bi_2Te_3 duo to its larger band gap and effective mass.[4] In the past ten years, many efforts were thrown into the fabrication of a p-type Bi_2Se_3 material, but only a few attempts were successful, e.g., the single crystal doped with Pb, Sb, Ca, and Mn with very low carrier concentration (1.63-2.66 $\times 10^{18}$ cm^{-3}),[5-7] and the poly-crystalline $Mg_{0.01}Bi_{1.99}Se_{3.06}$.[8] However, the Seebeck coefficient of $Mg_{0.01}Bi_{1.99}Se_{3.06}$ becomes negative at temperatures above 200 °C, and the thermoelectric performance of all reported p-type single crystal Bi_2Se_3-based materials were at low temperatures, thus the predication of Park and Singh is still an open question.

Generally, the manipulation of intrinsic defects is an important topic not only on thermoelectrics, but also on other functional materials, e.g., catalysts, functional oxide ceramics, optoelectronic materials. Specifically, strategies like self-compensation effect,[9,10] external doping,[11,12] chemical reduction,[13,14] and other approaches[15,16] were widely applied to regulate the intrinsic carriers' type or concentration. For Bi_2Se_3, the formation energies of both antisite defect (Bi_{Se}) and anion vacancy (V_{Bi}) are higher than those of Bi-Sb-Te materials,[3] which is due to the large atomic radius and electronegativity differences. Therefore, to achieve a p-type Bi_2Se_3-based thermoelectric material, we need to suppress the formation of Se vacancy (V_{Se}). In this work, we report an intrinsic p-type poly-crystalline $Bi_{0.8}Sb_{0.8}In_{0.4}Se_3$ through substituting large amount of Bi with In and Sb with the aim to increase the configurational entropy. The as-fabricated $Bi_{0.8}Sb_{0.8}In_{0.4}Se_3$ shows a rhombohedral crystalline structure with an intrinsic Seebeck coefficient of 500 $\mu V\ K^{-1}$ at room temperature. An optimized ZT of 0.48 at 350 °C is obtained by further adding Mn as an electron acceptor dopant.

Fig. 1(a) shows the XRD patterns of $BiSbSe_3$, $Bi_{0.9}SbIn_{0.1}Se_3$, $Bi_{0.8}SbIn_{0.2}Se_3$, $Bi_{0.6}SbIn_{0.4}Se_3$, and $Bi_{0.8}Sb_{0.8}In_{0.4}Se_3$. The poly-crystalline Bi_2Se_3 and its related compounds were synthesized by

using the 10 h ball milling (SPEX 8000D, SPEX SamplePrep LLC) and 5 min spark plasma sintering (SPS-211LX, Fuji Electronic Industry Co. Ltd). The peaks of pristine $BiSbSe_3$ well match the orthorhombic structure (PDF#15-0861 Sb_2Se_3) without impurity phases. However, after the introduction of In element into the $BiSbSe_3$ matrix with the stoichiometric reduction of Bi element, the main phase transforms into a rhombohedral structure with a space group of $R\bar{3}m$, same as that of Bi_2Te_3. Furthermore, this transformation is strengthened with the increase of In content, whereas single rhombohedral phase cannot be obtained by only manipulating the content of Bi and In. We find that further tuning of Sb content promotes this transformation, and pure rhombohedral structure phase is achieved in the sample $Bi_{0.8}Sb_{0.8}In_{0.4}Se_3$, showing that the increased configuration entropy can stabilize the rhombohderal phase. The refined lattice constants for pristine $Bi_{0.8}Sb_{0.8}In_{0.4}Se_3$ material are a = 4.061 Å and c = 28.783 Å, while for pristine Bi_2Se_3, a = 4.138 Å, c = 28.640 Å. It is seen that the c/a ratio increases from 6.97 (Bi_2Se_3) to 7.09 ($Bi_{0.8}Sb_{0.8}In_{0.4}Se_3$) by the alloying effect. Field-emission scanning electron microscopy (FE-SEM) imaging reveals that $Bi_{0.8}Sb_{0.8}In_{0.4}Se_3$ material shows randomly oriented lamellar features with grain size of 5-10 μm. EDS mapping results indicate that the elements are homogenously distributed in the matrix (Fig. S1) and no obvious secondary phase is observed, further supporting the single phase of $Bi_{0.8}Sb_{0.8}In_{0.4}Se_3$. Fig. 1(b) compares the Seebeck coefficients of pristine Bi_2Se_3, In_2Se_3,[17] $BiSbSe_3$,[18] and $Bi_{0.8}Sb_{0.8}In_{0.4}Se_3$. It is clear that the binary and ternary selenides exhibit n-type behavior from room temperature to 400 ℃, as their Seebeck coefficients are negative. However, the Seebeck coefficient of $Bi_{0.8}Sb_{0.8}In_{0.4}Se_3$ becomes positive in the whole temperature range (RT - 400 ℃), exhibiting an intrinsic p-type semiconductor behavior. In order to investigate the intrinsic p-type behavior, the precise elemental compositions of Bi_2Se_3-based selenides with rhombohedral structure were measured as listed in Table 1. The Se contents per formula are 2.91, 2.98, and 3.10 for Bi_2Se_3, $Bi_{1.6}Sb_{0.4}Se_3$, and $Bi_{0.8}Sb_{0.8}In_{0.4}Se_3$, respectively. It is noted that Bi site alloying with large amount of Sb and In significantly reduce the Se deficiency, suggesting that the increased configuration entropy (0 for Bi_2Se_3 to 1.05 k_B/f.u. for $Bi_{0.8}Sb_{0.8}In_{0.4}Se_3$, presented in Table 2) could be an effective approach to suppress the formation of the donor defect V_{Se}. This provides a new

guisdance to manipulate the defect concentration in other thermoelectrics via high entropy engineering.

It is noted that the as-fabricated p-type $Bi_{0.8}Sb_{0.8}In_{0.4}Se_3$ has an intrinsic low carrier concentration of ~10^{17} cm^{-3} as shown in Table 2, which is far from the optimized carrier concentration in the range of 10^{18}-10^{20} cm^{-3}.[19] Elemental doping is an effective approach to manipulate the carrier concentration and improve thermoelectric performance.[20] Mn dopant as a hole provider is applied in $Bi_{0.8}Sb_{0.8}In_{0.4}Se_3$. The XRD patterns of $Mn_xBi_{0.8-x}Sb_{0.8}In_{0.4}Se_3$ (x = 0.01, 0.02, 0.03, and 0.04) are well maintained, compared with that of $Bi_{0.8}Sb_{0.8}In_{0.4}Se_3$ (Fig. S2). Fig. 2 depicts the thermoelectric properties of the $Mn_xBi_{0.8-x}Sb_{0.8}In_{0.4}Se_3$ with different Mn doping contents. The room temperature electrical conductivity increases nearly two orders from 18 S m^{-1} through 2 × 10^3 S m^{-1}, 11 × 10^3 S m^{-1}, 13 × 10^3 S m^{-1} to 7 × 10^3 S m^{-1} as the Mn content increases from x = 0 through x = 0.01 to x = 0.04, respectively, indicating that Mn is an effective electron acceptor (Fig. 2(a)). It is clearly seen that the carrier concentration increases by more than two orders from 10^{17} cm^{-3} to 10^{20}-10^{21} cm^{-3} for Mn doped samples, while the carrier mobility experiences a slight change varied from 4 cm^2 V^{-1} s^{-1} to 8 cm^2 V^{-1} s^{-1} (Table 2). A high carrier concentration in the degenerated range is necessary to suppress the intrinsic excitation. Fig. 2(b) shows the temperature dependent Seebeck coefficients of pristine and Mn doped samples. The Seebeck coefficients of all Mn doped samples are positive, exhibiting p-type behavior. The room temperature Seebeck coefficients decrease from 500 μV K^{-1}, through 197 μV K^{-1}, 141 μV K^{-1}, 137 μV K^{-1} to 141 μV K^{-1} as the Mn content increases from x = 0 through to x = 0.01 to 0.04, respectively, resulting from the increased carrier concentration. The temperature dependent electrical conductivity and Seebeck coefficients suggest that all Mn doped samples are already degenerated, showing a decreasing σ and increasing S as temperature rises.

Owing to the optimized carrier concentration, the power factor of all the $Mn_xBi_{0.8-x}Sb_{0.8}In_{0.4}Se_3$ samples has increased in the whole temperature range, as presented in Fig. 2(c). A peak power factor of ~420 μW m^{-1} K^{-2} at 250 °C is obtained in $Mn_{0.03}Bi_{0.77}Sb_{0.8}In_{0.4}Se_3$, which is about 2000% higher than that of the pristine $Bi_{0.8}Sb_{0.8}In_{0.4}Se_3$. We have also calculated the Pisarenko curve based

on the single parabolic band (SPB) model[21] with the effective mass m^*/m_0 = 0.5, 1.5 or 2.0 as displayed in Fig. 2(d). It is clearly seen that $Bi_{0.8-x}Mn_xSb_{0.8}In_{0.4}Se_3$ (1.5-2.0 m_0) has a much higher effective mass than Bi_2Se_3 (0.5 m_0), suggesting different band edge structures.

We then perform density functional theory (DFT) calculations to obtain the band structures of Bi_2Se_3 and $Bi_{0.8}Sb_{0.8}In_{0.4}Se_3$ (see supplementary information for computational details), as shown in Fig. 3. The crystal structure of Bi_2Se_3 is schematically drawn in Fig. 3(a). It is seen from Fig. 3(c, d) that the effective mass of the valence band maximum (VBM) at Γ point is larger in $Bi_{0.8}Sb_{0.8}In_{0.4}Se_3$ as the band becomes more flattened.[22,23] The increased band effective mass results in a low carrier mobility, as μ is proportional to $1/m_b^*$,[22] which is also observed in our samples as shown in Table 2. The energies of additional carrier pockets (ACP) between Z-F (N_v = 6) and L point (N_v = 3)[24,25] also increase as the energy difference $\Delta E_{\Gamma\text{-}ZF}$ ($\Delta E_{\Gamma\text{-}L}$) decreases from 0.26 eV (0.43 eV) to 0.02 eV (0.14 eV). According the $5k_BT$ rule,[26] those additional carrier pockets could contribute to the thermoelectric transport, especially in the high temperature range, which results in an enhanced effective mass as the increase of carrier concentration. Generally, the as-fabricated $Mn_xBi_{0.8-x}Sb_{0.8}In_{0.4}Se_3$ materials have a multiple band conduction behavior, which is of great benefit to the electrical transport properties.

Fig. 4(a) shows the temperature dependent thermal conductivity of pristine and Mn doped samples. The room temperature thermal conductivity increases from 0.56 W m^{-1} K^{-1} to 0.67 W m^{-1} K^{-1} as Mn dopant increases from 0 to 0.03 due to the increased electronic thermal conductivity κ_e, obtained using the Wiedemann-Franz relationship $\kappa_e = L\sigma T$, where L is Lorentz number. For pristine $Bi_{0.8}Sb_{0.8}In_{0.4}Se_3$, it shows a notable bipolar effect near 250 ℃ due to the intrinsic low carrier concentration. With the much increase of the carrier concentration, the bipolar thermal conductivity can be significantly suppressed,[27,28] leading to a continuous reduction of the total thermal conductivities of $Mn_{0.03}Bi_{0.77}Sb_{0.8}In_{0.4}Se_3$ and $Mn_{0.04}Bi_{0.76}Sb_{0.8}In_{0.4}Se_3$ samples. Comparing to $Bi_{0.8}Sb_{0.8}In_{0.4}Se_3$, the thermal conductivities of $Mn_{0.03}Bi_{0.77}Sb_{0.8}In_{0.4}Se_3$ and $Mn_{0.04}Bi_{0.76}Sb_{0.8}In_{0.4}Se_3$ decrease about 5.6% and 7.5 %, respectively, at 400 ℃. Fig. 4(b) presents the dimensionless figure of merit as a function of temperature for $Mn_xBi_{0.8-x}Sb_{0.8}In_{0.4}Se_3$. It is clearly

seen that all Mn doped samples have increased ZT values in the whole temperature range and the peak value is pushed to higher temperatures as compared with the undoped one. A maximum ZT value of ~0.48 is achieved in $Mn_{0.03}Bi_{0.77}Sb_{0.8}In_{0.4}Se_3$ at 350 ℃, even larger than that of the reported n-type Bi_2Se_3.[18] Although this value is still humble as compared with other p-type thermoelectric materials, e.g., Cu_2Se, PbSe and SnSe, it can be a good starting point to explore other p-type Bi_2Se_3-like selenides.

In summary, we successfully manipulate the intrinsic defect of Bi_2Se_3-based materials and achieve a robust p-type Te-free thermoelectric material $Bi_{0.8}Sb_{0.8}In_{0.4}Se_3$ in its polycrystalline form. The band convergency induced by alloying Sb and In at Bi site leads to a relatively high positive Seebeck coefficient. Further optimization of carrier concentration by Mn dopant synergistically promotes the electrical properties and suppresses the bipolar effect, achieving a high ZT value of ~0.48 at 350 ℃. Our work introduces a robust Te-free p-type polycrystalline Bi_2Se_3-based thermoelectric material and evaluates its thermoelectric properties at medium temperatures, providing a new insight into manipulating the intrinsic defects of other classic thermoelectric materials via high entropy strategy.

See the supplementary material for details of computation and experiment. The XRD patterns and refined lattice constants, Hall carrier concentration and carrier mobility, and the specific heat capacity of $Mn_xBi_{0.8-x}Sb_{0.8}In_{0.4}Se_3$ and Bi_2Se_3 are also presented.

ACKNOWLEDGMENTS

This work was supported by the National Key Research and Development Program of China [grant number 2018YFB0703600], ECF under project [grant number 69/2018] and the Tencent Foundation through the XPLORER PRIZE. The theoretical calculations are supported by the research computing facilities offered by ITS, HKU.

DATA AVAILABILITY

All data generated or analyzed in this study are included in this published article and its supplementary material.

REFERENCES

[1]S. Urazhdin, D. Bile, S. H. Tessmer, and S. D. Mahanti, Phys. Rev. B **66**, 161306 (2002).

[2]S. X. Wang, and P. Zhang, Phys. Lett. A **384**, 126281 (2020).

[3]L. P. Hu, T. J. Zhu, X. H. Liu, and X. B. Zhao, Adv. Funct. Mater. **24**, 5211 (2014).

[4]D. Park, and D. J. Singh, Phys. Rev. X **1**, 21005 (2010).

[5]J. Kašparová, Č Drašar, A. Krejčová, L. Beneš, P. Lošťák, W. Chen, Z. H. Zhou, and C. Uher, J. Appl. Phys. **97**, 103720 (2005).

[6]Z. Y. Wang, T. Lin, P, Wei, X. F. Liu, R. Dumas, K. Liu, and J. Sui, Appl. Phys. Lett. **97**, 042112 (2010).

[7]Y. H. Choi, N. H. Jo, K. J. Lee, H. W. Lee, Y. H. Jo, J. Kajino, T. Takabatake, K. T. Ko, J. H. Park, and M. H. Jung, Appl. Phys. Lett. **101**, 152103 (2012).

[8]J. Andoulakis, and E. Beciragic, Solid State Commun. **173**, 5 (2013).

[9]J. W. Zhang, L. R. Song, G. K. Madsen, K. F. Fischer, W. Q. Zhang, X. Shi, and B. B. Iversen, Nat. Commun. **7**, 10892 (2016).

[10]Y.B. Zhu, Z.J. Han, F. Jiang, E.T. Dong, B.-P. Zhang, W.Q. Zhang, and W.S. Liu, Mater. Today Phys. **16**, 100327 (2021).

[11]W.-S. Liu, B.-P. Zhang, L.-D. Zhao, and J.-F. Li, Chem. Mater. **20**, 7526 (2008).

[12]X.W. Zhang, Y. Wang, and L.T. Li, Ferroelectrics. **101**, 61 (1990).

[13]D.F. Yan, Y.X. Li, J. Huo, R. Chen, L.M. Dai, and S.Y. Wang, Adv. Mater. **29**, 1606459 (2017).

[14]J. Di, J.X. Xia, X.W. Li, M. X. Ji, H. Xu, Z.G. Chen, and H.M. Li, Carbon **107**, 1 (2016).

[15]Y. Pan, T.-R. Wei, C.-F. Wu, and J.-F. Li, J. Mater. Chem. C **3**, 10583 (2015).

[16]T.J. Zhu, L.P. Hu, X.B. Zhao, and J. He, Adv. Sci. **3**, 1600004 (2016).

[17]J.L. Cui, X.L. Liu, X.J. Zhang, Y.Y. Li, and Y. Deng, J. Appl. Phys. **110**, 023708 (2011).

[18]X. Y. Liu, D. Y. Wang, H. J. Wu, J. F. Wang, Y. Zhang, G. T. Wang, S. J. Pennycook, and L.-D. Zhao, Adv. Funct. Mater. **29**, 1806558 (2019).

[19]Y. Z. Pei, A. D. LaLonde, N. A. Heinz, X. Y. Shi, S. H. Lwanaga, H. Wang, L. D. Chen, and G. J. Snyder, Adv. Mater. **23**, 5674 (2011).

[20]G.-H. Kim, L. Shao, K. Zhang, and K.P. Pipe, Nat. Mater. **12**, 719 (2013).

[21]W.S. Liu, J.W. Zhou, Q. Jie, Y. Li, H.S. Kim, J.M. Bao, G. Chen, and Z.F. Ren, Energy Environ. Sci. **9**, 530 (2016).

[22]Y. Z. Pei, X. Y. Shi, A. LaLonde, H. Wang, L. D. Chen, and G. J. Snyder, Nature **473**, 66 (2011).

[23]H. Usul, and K. Kuroki, J. Appl. Phys. **121**, 165107 (2017).

[24]T. Fang, X. Li, C.L. Hu, Q. Zhang, J. Yang, W.Q. Zhang, X.B. Zhao, D.J. Singh, and T.J. Zhu, Adv. Funct. Mater. **29**, 1900677 (2019).

[25]G.F. Wang, and T. Cagin, Phys. Rev. B **76**, 075201 (2007).

[26]W.-S. Liu, L.-D. Zhao, B.-P. Zhang, H.-L Zhang, and J.-F. Li, Appl. Phys. Lett. **93**, 042109 (2008).

[27]W.-S. Liu, B.-P. Zhang, J.-F. Li, H.-L. Zhang, and L.-D. Zhao, J. Apply. Phys. **102**, 103717 (2007).

[28]H.X. Qin, Y. Liu, Z.W. Zhang, Y.M. Wang, J. Cao, W. Cai, Q. Zhang, and J.H. Sui, Mater. Today Phys. **6**, 31 (2018).

FIGURES

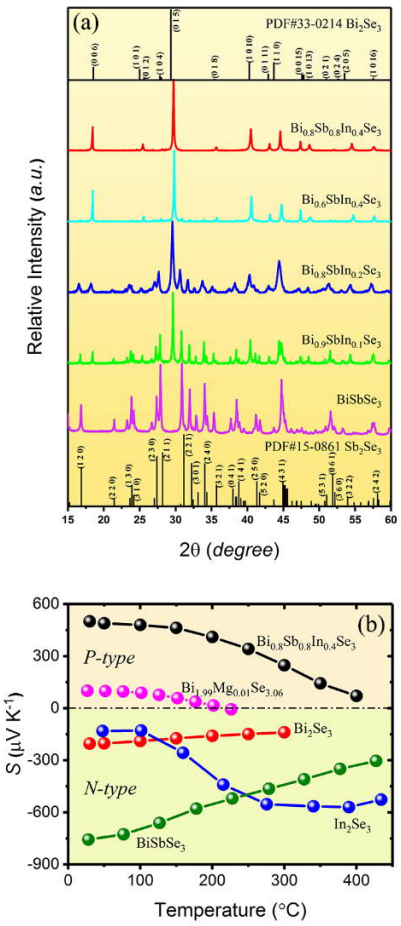

FIG. 1. (a) XRD patterns of $BiSbSe_3$, $Bi_{0.9}SbIn_{0.1}Se_3$, $Bi_{0.8}SbIn_{0.2}Se_3$, $Bi_{0.6}SbIn_{0.4}Se_3$, and $Bi_{0.8}Sb_{0.8}In_{0.4}Se_3$. (b) Seebeck coefficients of pristine Bi_2Se_3, In_2Se_3[17], $BiSbSe_3$[18], $Bi_{0.8}Sb_{0.8}In_{0.4}Se_3$, and $Bi_{1.99}Mg_{0.01}Se_{3.06}$[8].

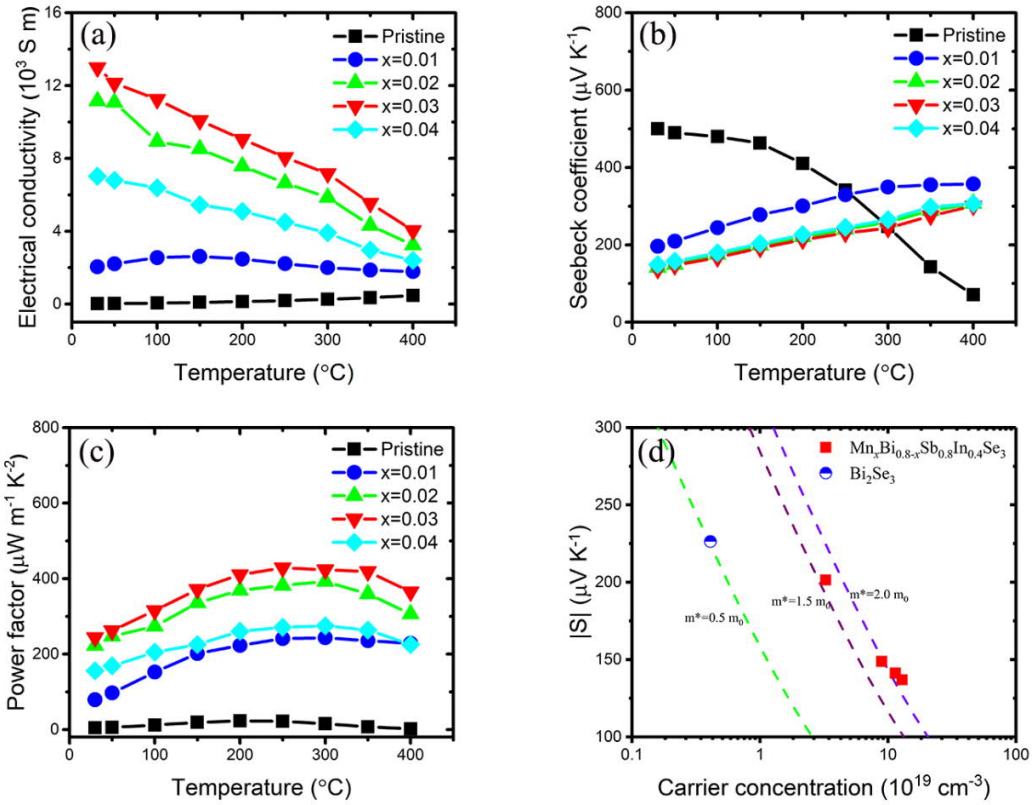

FIG. 2. Temperature dependent (a) electrical resistivity, (b) Seebeck coefficient, and (c) power factor for $Mn_xBi_{0.8-x}Sb_{0.8}In_{0.4}Se_3$ samples (x = 0, 0.01, 0.02, 0.03, and 0.04). (d) The absolute value of Seebeck coefficient as a function of Hall carrier concentration for Bi_2Se_3[18] and $Mn_xBi_{0.8-x}Sb_{0.8}In_{0.4}Se_3$ samples (x = 0.01, 0.02, 0.03, and 0.04). The dashed line is plotted according to Pisarenko line with effective mass m^*/m_0 = 0.5, 1.5, or 2.0.

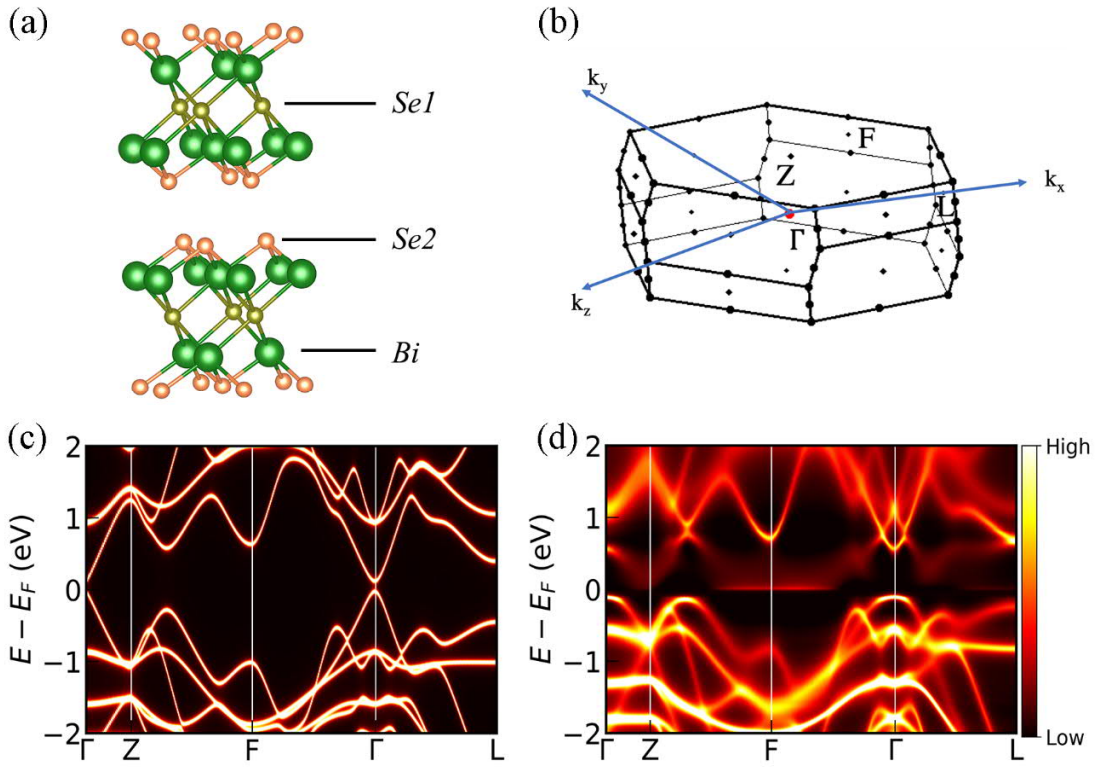

FIG. 3. (a) Schematic crystal structure and (b) Brillouin zone of Bi_2Se_3. Bloch spectral functions of (c) Bi_2Se_3 and (d) $Bi_{0.8}Sb_{0.8}In_{0.4}Se_3$ calculated using the KKR-CPA method. E_F represents Fermi energy.

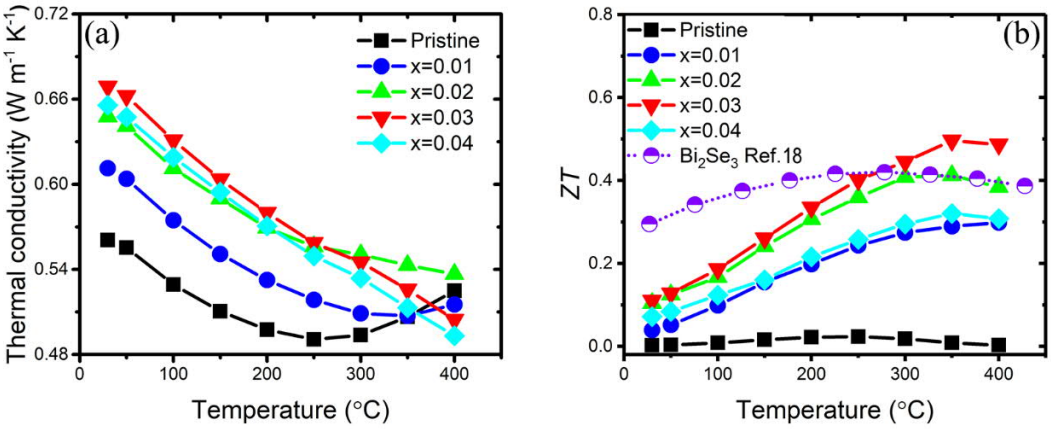

FIG. 4. Temperature dependent (a) thermal conductivity, and (b) ZT value of $Mn_xBi_{0.8-x}Sb_{0.8}In_{0.4}Se_3$ samples (x = 0, 0.01, 0.02, 0.03, and 0.04).

TABLE 1. Elemental compositions and configurational entropies of selected selenides with rhombohedral crystal structure.

Compounds	Bi	Sb	In	Se	**Configurational Entropy (k_B/f.u.)**
Bi_2Se_3	2.0000	-	-	2.9087	0
$Bi_{1.6}Sb_{0.4}Se_3$	1.6112	0.3888	-	2.9766	0.50
$Bi_{0.8}Sb_{0.8}In_{0.4}Se_3$	0.8039	0.8063	0.3898	3.1028	1.05

TABLE 2. Hall carrier concentration (n) and carrier mobility (μ) of $Mn_xBi_{0.8-x}Sb_{0.8}In_{0.4}Se_3$ and Bi_2Se_3[18] at room temperature.

$Mn_xBi_{0.8-x}Sb_{0.8}In_{0.4}Se_3$	$x = 0$	$x = 0.01$	$x = 0.02$	$x = 0.03$	$x = 0.04$	Bi_2Se_3[18]
n (10^{19} cm^{-3})	0.019	3.259	8.906	12.857	11.340	0.41
μ (cm^2 V^{-1} s^{-1})	5.88	6.38	7.54	5.99	3.87	566